

# Scattering in the $\pi N$ negative parity channel in lattice QCD

C. B. Lang<sup>1,\*</sup> and V. Verduci<sup>1,†</sup>

<sup>1</sup>*Institut für Physik, FB Theoretische Physik, Universität Graz, A-8010 Graz, Austria*

(Dated: September 17, 2018)

We study the coupled  $\pi N$  system (negative parity, isospin  $\frac{1}{2}$ ) based on a lattice QCD simulation for  $n_f=2$  mass degenerate light quarks. Both, standard 3-quarks baryon operators as well as meson-baryon (4+1)-quark operators are included. This is an exploratory study for just one lattice size and lattice spacing and at a pion mass of 266 MeV. Using the distillation method and variational analysis we determine energy levels of the lowest eigenstates. Comparison with the results of simple 3-quark correlation studies exhibits drastic differences and a new level appears. A clearer picture of the negative parity nucleon spectrum emerges. For the parameters of the simulation we may assume elastic  $s$ -wave scattering and can derive values of the phase shift.

PACS numbers: 11.15.Ha, 12.38.Gc

## I. INTRODUCTION

Even if we consider only strong interactions almost all hadrons are unstable. Calculations in lattice Quantum Chromodynamics (QCD) should therefore take into account the resonant nature of these states and the coupled decay channels. The bulk of lattice studies rely on correlation functions for simple  $\bar{q}q$  or  $qqq$ -type operators for mesons or baryons, respectively. Formally one would expect that in the full quantum field theory with dynamical quarks these simple meson or baryon operators should (via dynamical vacuum loops) couple to meson-meson or meson-baryon states. It was found that such intermediate channels seem to be coupling too weak to be observed (see, e.g., [1–7] for baryon correlation studies). Therefore one needs to include explicitly hadron-hadron operators in the set of interpolators, as has been demonstrated in meson resonance studies [8–14].

The interplay between resonance levels and hadron-hadron states has been discussed in [15–18], where the resulting energy levels for finite spatial volume were related to the continuum scattering phase shift in the elastic region. Comparing the energy levels of a non-interacting hadron-hadron state with those in the case of interactions one finds a significant level shift (“avoided level crossing”) in the energy region of the resonance. The effect of such coupled channels depends on the system parameters. For small volumes and unphysical large quark masses the two-hadron energy levels may lie high above the observed resonance levels or - for narrow resonances - outside the influence region of the resonance.

Often it is technically not possible (e.g., due to a small volume) to determine more than a few lowest energy levels below the elastic threshold. In the elastic scattering region each energy level corresponds to one value of the phase shift and the resonance region then cannot be mapped out sufficiently well. On the other hand, each

change of volume or other parameters requires a completely new simulation sequence (i.e., generating configurations with dynamical fermions, quark propagators etc.) Studying interpolators in moving frames [19–23] allows to obtain further values on the same configurations. Unfortunately, for coupled channels with two hadrons of different mass, there can be mixing between different partial waves, complicating the situation. Another complication is the opening of inelastic channels.

Starting from continuum models for a scattering process, based on phenomenologically determined parameters, one can also derive the energy levels on finite volume lattices [24–27]. Coupled channel potential models or Unitarized Chiral Perturbation Theory motivated models in that way allow to compare with lattice results. Alternative methods to identify resonance parameters have been discussed in that context [24, 28, 29].

A particularly interesting case is the negative parity nucleon channel. There we have two low lying resonances  $N^*(1535)$  and  $N^*(1650)$  which couple to  $N\pi$  in  $s$ -wave. Above the 10% level there are also further inelastic decays  $N^*(1535) \rightarrow N\eta$  and  $N^*(1650) \rightarrow N\eta, \Lambda K$ . So far lattice simulations of this channel, that have determined ground state energy levels and further excitations, included only 3-quark interpolators [4–7]. In these studies two low lying energy levels have been identified and assigned to the two negative parity resonances. However, the lower of the two levels showed a tendency to lie below the  $N^*(1535)$ .

In order to clarify the situation we study here for the first time the coupled system of 3-quark nucleon interpolators and pion-nucleon interpolators in the negative parity channel. The calculation requires the computation of many more correlation graphs than before, including the notoriously demanding backtracking quark line contributions. We therefore use the distillation method [30] for determining the cross correlation matrix for up to 9 interpolators. We use gauge configurations with  $n_f = 2$  mass degenerate dynamical quarks (of improved Wilson type) with a pion mass of 266 MeV. The  $16^3 \times 32$  lattices have spatial extent of 1.98 fm with  $Lm_\pi \approx 2.68$  (for details see Table I). The energy levels are obtained with the variational method [15, 31–33].

\*Electronic address: christian.lang@uni-graz.at

†Electronic address: valentina.verduci@uni-graz.at

$N_S^3 \times N_T$	$\beta$	$a[\text{fm}]$	$L[\text{fm}]$	$Lm_\pi$	#configs	$m_\pi[\text{MeV}]$
$16^3 \times 32$	7.1	0.1239(13)	1.98	2.68	280	266(3)(3)

TABLE I: Configurations used for the present study.  $N_S$  and  $N_T$  denote the number of lattice points in spatial and time directions, and  $L = N_S a$  is the size in physical units.

The energy levels of the eigenstates in case of a finite spatial extent  $L$  are discrete. They are determined by diagonalizing the correlation matrix of interpolating operators. The set of these interpolators has to be large enough to allow the representation of the eigenstates. For total momentum zero the pion-nucleon operators will have the form  $N(n)\pi(-n)$  where  $n$  abbreviates the possible quantized momentum values  $2n\pi/L$ . For the non-interacting situation the corresponding energies are straightforward to compute, for the interacting case they are shifted and have to be determined numerically from the correlation matrix. We need to consider all interpolators that may couple to the system in the energy region where one expects eigenstates. Obviously the 3-quark interpolators and the interpolator  $N(0)\pi(0)$  have to be included. In our setting already the  $s$ -wave operator  $N(1)\pi(-1)$  lies high above the lowest energy level. The same holds for a possible  $N\eta_2$  channel (note, that for only two dynamical quarks there is just one  $\eta$  meson called  $\eta_2$ ). We find that the spectrum shows a clear difference whether the pion-nucleon operator is included or not. If the pion-nucleon interpolator is included we observe one more level below threshold, typical for attractive channels, and the next two levels are shifted closer to the expected resonances.

Following Sect. II where we present the parameters and methods used, we discuss the results in Sect. III. The appendix lists the necessary Wick contractions for the meson-baryon correlators.

## II. METHODS

### A. Lattice action and configurations

We use configurations from the study of re-weighting techniques [34, 35] generously provided by the authors. The gauge configurations were generated for  $n_f = 2$  flavors of mass-degenerate light quarks and a tree level improved Wilson-Clover action with gauge links smeared using one level of normalized hypercubic smearing (nHYP smearing). The valence u/d quarks have the same mass as the sea u/d quarks. Table I lists the parameters used for the simulation along with the number of (approximately independent) gauge configurations used, the lattice spacing, volume and the pion mass (for details see [8, 11]). We note that the small value  $Lm_\pi \approx 2.68$  may lead to finite size effects which we cannot identify in this study, since we have just one lattice size available.

### B. Determination of energy levels

Due to the finiteness of the spatial volume, the energy spectrum of the correlation functions is discrete. We determine the energy levels of the  $N$  and the  $N\pi$  system with the variational method [15, 31–33]. For a given quantum channel one measures the Euclidean cross-correlation matrix  $C(t)$  between several interpolators,

$$C_{ij}(t) = \langle O_i(t) \bar{O}_j(0) \rangle = \sum_n \langle O_i(t) | n \rangle e^{-E_n t} \langle n | \bar{O}_j(0) \rangle, \quad (1)$$

where the operators are located on the corresponding Euclidean time slices. The generalized eigenvalue problem  $C(t)\vec{u}_n(t) = \lambda_n(t)C(t_0)\vec{u}_n(t)$  disentangles the eigenstates  $|n\rangle$  with the eigenvalues

$$\lambda_n(t, t_0) = e^{-E_n(t-t_0)} \left( 1 + \mathcal{O}\left(e^{-\Delta E_n(t-t_0)}\right) \right), \quad (2)$$

where  $\Delta E$  may be as small as the distance to the next nearby energy level. From the exponential decay one determines the energy values of the eigenstates by exponential fits. The stability of the eigenvectors with regard to  $t$  and the so-called effective energies

$$E_n(t) = \log \frac{\lambda_n(t)}{\lambda_n(t+1)} \quad (3)$$

indicate the suitable fit range by exhibiting plateau-like behavior. The set of interpolators should be large enough to allow the system to reproduce the physical eigenstates. Neglecting important interpolators may obscure the result. On the other hand, in the calculations it is not possible to have a complete set of interpolators and one is limited to a reasonable subset. Also, the statistical quality of  $C(t)$  is an issue. The reliability of the obtained energy levels decreases for higher  $|n\rangle$ , with the ground state being the most reliable one.

The energy values are extracted using correlated fits of  $\lambda_n(t)$  to one and two exponentials. A possible source of systematic error is the choice of the fit range in  $t$ . From the effective energy plots (cf., Figs. 2 and 3), the range of stability of the eigenvectors and the  $\chi^2$  dependence of the fits we estimate suitable fit ranges. The two exponential fits start at smaller  $t$  and we verify that the extracted levels agree with results obtained from one-exponential fits starting at larger  $t$ .

### C. Interpolators

The  $N\pi$  system can be projected to isospin  $\frac{1}{2}$  and  $\frac{3}{2}$ , experimentally accessible by  $\pi^\pm p$  scattering. Here we study only the isospin  $\frac{1}{2}$  sector.

For the charged nucleon interpolator we use the oper-

ator (on a given time slice)

$$(N_{\pm}^{(i)})_{\mu}(\vec{p}=0) = \sum_{\vec{x}} \epsilon_{abc} \left( P_{\pm} \Gamma_1^{(i)} u_a(\vec{x}) \right)_{\mu} \left( u_b^T(\vec{x}) \Gamma_2^{(i)} d_c(\vec{x}) \right), \quad (4)$$

and for the neutral one with the quarks  $d, u, d$ . ( $\Gamma_1, \Gamma_2$ ) can assume the three values ( $\mathbf{1}, C\gamma_5$ ), ( $\gamma_5, C$ ) and ( $i\mathbf{1}, C\gamma_t\gamma_5$ ) for  $i = 1, 2, 3$ .  $C$  denotes the charge conjugation matrix,  $\gamma_t$  the Dirac matrix in time direction, and  $P_{\pm} = \frac{1}{2}(1 \pm \gamma_t)$  the parity projector. We sum over all points of the time slice in order to project to zero momentum. Summation over the color indices  $a, b, c$  and the (not shown) Dirac indices is implied.

In the distillation approach (see Subsect. IID below) the sources are smeared combining  $N_v$  eigenvectors. For the nucleon 3-quark interpolators we choose  $N_v = 32$  and  $N_v = 64$  and thus with the three different Dirac structures have six operators.

The pion interpolators read

$$\begin{aligned} \pi^+(\vec{p}=0) &= \sum_{\vec{x}} \bar{d}_a(\vec{x}) \gamma_5 u_a(\vec{x}), \\ \pi^0(\vec{p}=0) &= \sum_{\vec{x}} \frac{1}{\sqrt{2}} (\bar{u}_a(\vec{x}) \gamma_5 u_a(\vec{x}) - \bar{d}_a(\vec{x}) \gamma_5 d_a(\vec{x})), \end{aligned} \quad (5)$$

where summation over the color index  $a$  is implied.

We consider the  $N\pi$  system in the rest frame. The leading  $s$ -wave contribution then comes from the interpolator with both particles at rest,

$$N\pi(\vec{p}=0) = \gamma_5 N_+(\vec{p}=0) \pi(\vec{p}=0), \quad (6)$$

where  $N_+$  denotes the positive parity nucleon and the factor  $\gamma_5$  ensures negative parity for the interpolator. In the distillation approach we choose for the  $N\pi$  channel  $N_v = 32$  and thus with the three different nucleon interpolators have three operators.

We project to isospin  $\frac{1}{2}$  by choosing the combination

$$O_{N\pi}(I = \frac{1}{2}, I_3 = \frac{1}{2}) = p\pi^0 + \sqrt{2}n\pi^+, \quad (7)$$

with  $p$  and  $n$  denoting the charged and the neutral nucleon according to (4).

The negative parity  $N^*$  channel becomes quickly inelastic (see, e.g., [36–39]). According to the Particle Data Group [40] the main decay channel is  $N\pi$  (35-55% for  $N^*(1535)$ , 50-90 % for  $N^*(1650)$ ). The second largest decay rate is to  $N\eta$  (42±10% for  $N^*(1535)$ , 5-15 % for  $N^*(1650)$ ). Most of the rest of 10-20 % is  $N\pi\pi$  and, for  $N^*(1650)$ , also  $\Lambda K$ . For a lattice calculation at physical quark masses one would need to include the inelastic channels. This is beyond present days capacities.

In our case ( $n_f = 2$ ) there is just one pseudoscalar meson  $\eta$  called  $\eta_2$ , with a mass larger than 800 MeV [41, 42]. With our parameters (see Sect. III) these inelastic

channels would thus have thresholds above 1900 MeV. The lowest state with total momentum zero but non-zero relative momentum  $N(1)\pi(-1)$  (momentum units  $2\pi/(16a)$ ) has a (non-interacting) energy of 1920 MeV, as well. These energy values are above the observed lowest three levels. We cannot exclude that in particular the highest of these may be influenced by the  $N(1)\pi(-1)$  state.

#### D. Distillation method and correlation function

We compute the correlation matrix entries with help of the distillation method [30]. This method has been successfully applied in several studies, including baryon correlation functions [3, 4, 8, 11, 12, 43, 44]. It also allows for a reliable evaluation of the partially disconnected diagrams. On a given time slice one introduces separable (i.e., expressed by a sum of products separating the dependence on  $\vec{x}$  and  $\vec{x}'$ ) quark smearing sources in the form

$$\begin{aligned} q_{c,\alpha}(\vec{x}) &\rightarrow \sum_{\vec{x}'} S_{cd}(\vec{x}, \vec{x}') q_{d,\alpha}(\vec{x}') \\ &\equiv \sum_{\vec{x}'} \sum_i^{N_v} v_c^i(\vec{x}) v_d^{i*}(\vec{x}') q_{d,\alpha}(\vec{x}'), \end{aligned} \quad (8)$$

where  $c, d$  and  $\alpha$  denote color and Dirac indices and summation over the color indices is implied. A suitable choice for the  $v^i$  is the eigenvectors of the spatial lattice Laplacian [30]. Summing over all eigenvectors reproduces the delta function, the spectral representation of unity. In actual calculation one truncates the sum and uses the lowest eigenmodes or subsets. The value of  $N_v$  depends on the lattice size and  $N_v$  between 32 and 96 was found suitable for our situation [8].

The advantage of the distillation approach lies in its versatility. Instead of quark propagators  $G_{c\mu; d\nu}(x, x_0)$  from one source located in  $x_0$  to other points on the lattice one now computes propagators between eigenmode sources, so-called perambulators

$$\tau_{\mu\nu}(j, t_{\text{snk}}; i, t_{\text{src}}) \equiv \sum_{\vec{x}, \vec{y}, c, d} v_d^{j*}(\vec{x}, t_{\text{snk}}) G_{d\mu; c\nu}(\vec{x}, \vec{y}) v_c^i(\vec{y}, t_{\text{src}}). \quad (9)$$

The interpolator structure decouples from the calculation of the perambulators completely. E.g., meson correlators assume the form

$$\begin{aligned} C(t_{\text{snk}}, t_{\text{src}}) &= \langle M(t_{\text{snk}}) M^\dagger(t_{\text{src}}) \rangle \\ &= \phi_{\mu\nu}(n, k; t_{\text{src}}) \tau_{\nu\alpha}(k, t_{\text{src}}; i, t_{\text{snk}}) \\ &\quad \phi_{\alpha\beta}(i, j; t_{\text{snk}}) \tau_{\beta\mu}(j, t_{\text{snk}}; n, t_{\text{src}}), \end{aligned} \quad (10)$$

where  $M$  denotes a meson interpolator like, e.g., the pion of Eq. (5) and summation over the source index ( $i, j, k, n$ ) pairs and the Dirac index ( $\alpha, \beta, \mu, \nu$ ) pairs is implied.

Due to  $\gamma_5$ -hermiticity of the Dirac operator the perambulator for sink to source can be expressed by that from source to sink,

$$\tau_{\nu\alpha}(k, t_{\text{src}}; i, t_{\text{snk}}) = \gamma_{5,\alpha\alpha'} \tau_{\alpha'\nu'}^\dagger(i, t_{\text{snk}}; k, t_{\text{src}}) \gamma_{5,\nu'\nu}. \quad (11)$$

The meson interpolator type is specified in

$$\begin{aligned} \phi_{\alpha\beta}(i, j; t) &= D_{\alpha\beta} \sum_{\vec{x}, \vec{y}} v_d^{i*}(\vec{y}) F_{dc}(\vec{y}, \vec{x}) v_c^j(\vec{x}) \\ &\equiv D_{\alpha\beta} \widehat{\phi}(i, j; t). \end{aligned} \quad (12)$$

The factors  $D$  and  $F$  represent the Dirac structure and momentum projection or derivative terms related to the quantum numbers of the meson. Only  $\phi$  has to be recomputed for each meson interpolator whereas the perambulator remains the same.

For 3-quark interpolators like the baryons one obtains contributions to the correlation function of the form

$$\begin{aligned} C_{\mu\nu}(t_{\text{snk}}, t_{\text{src}}) &= \langle N_\mu(t_{\text{snk}}) \overline{N}_\nu(t_{\text{src}}) \rangle \\ &= \phi_{\mu\alpha\beta\gamma}(i, j, k; t_{\text{snk}}) \\ &\quad \tau_{\alpha\alpha'}(i, t_{\text{snk}}; i', t_{\text{src}}) \\ &\quad \tau_{\beta\beta'}(j, t_{\text{snk}}; j', t_{\text{src}}) \\ &\quad \tau_{\gamma\gamma'}(k, t_{\text{snk}}; k', t_{\text{src}}) \\ &\quad \phi_{\nu\alpha'\beta'\gamma'}^\dagger(i', j', k'; t_{\text{src}}). \end{aligned} \quad (13)$$

For an interpolator  $N$  (without derivatives)  $\phi$  assumes the form

$$\begin{aligned} \phi_{\nu\alpha\beta\gamma}(i, j, k; t) &= D_{\nu\alpha\beta\gamma} \sum_{\vec{x}} \epsilon_{abc} v_a^i(\vec{x}) v_b^j(\vec{x}) v_c^k(\vec{x}) F(\vec{x}) \\ &\equiv D_{\nu\alpha\beta\gamma} \widehat{\phi}(i, j, k; t). \end{aligned} \quad (14)$$

Again,  $D$  carries the Dirac structure and  $F$  the possible total momentum projection factors.

We also project the correlation functions to definite parity with the projection operators  $P_\pm = \frac{1}{2}(1 \pm \gamma_t)$ . In App. A we list the necessary contraction terms expressed in terms of the perambulators.

### E. Energy levels: interpretation

We study the  $N\pi$  system in the  $\frac{1}{2}^-$  channel in  $s$ -wave in the rest frame. From the energy value

$$E = \sqrt{s} = \sqrt{(p_N + p_\pi)^2} = \sqrt{p^{*2} + m_\pi^2} + \sqrt{p^{*2} + m_N^2} \quad (15)$$

we extract the momentum  $p^* = |\mathbf{p}^*|$  with

$$p^{*2} = \frac{[s - (m_N + m_\pi)^2][s - (m_N - m_\pi)^2]}{4s}, \quad (16)$$

and the dimensionless product of the momentum and the spatial lattice size

$$q = p^* \frac{L}{2\pi}. \quad (17)$$

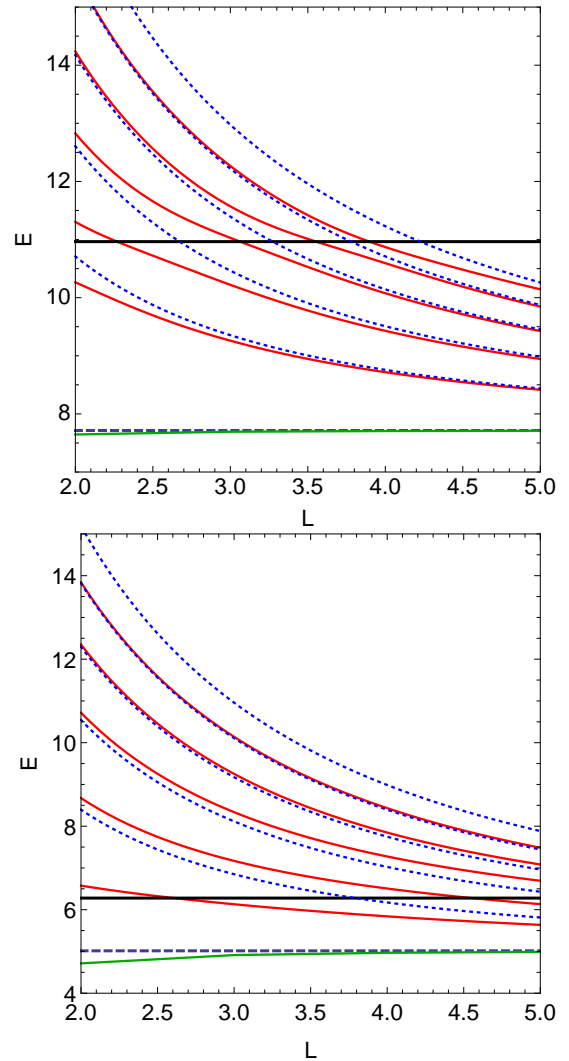


FIG. 1: Lowest energy levels vs. the spatial lattice size (both in units of the pion mass). Upper plot: physical pion, nucleon and  $N^*(1535)$  masses, comparing the non-interacting levels (dotted) with the levels distorted due to interaction (full lines); the broken horizontal line indicates the threshold, the horizontal thick line the  $N^*(1535)$ -mass; the  $N^*$  is parametrized as an elastic resonance with a decay width of 150 MeV. Lower plot: Unphysical values for  $m_\pi = 266$  MeV,  $m_N = 1068$  MeV; for  $N^*$  the mass is chosen as 1670 MeV without changing the coupling strength. In both cases the lowest possible state is  $N(0)\pi(0)$ , which coincides with the threshold in the non-interacting case. For attractive interaction the level moves slightly below the threshold to negative  $q^2$ .

For a system of non-interacting pions and nucleons the energy levels for given lattice size can be straightforwardly computed (dotted lines in Fig. 1). For the interacting case, with localized interaction region and in the elastic domain, Lüscher [15–18] has given a relation

between energy levels and phase shift,

$$\tan \delta(q) = \frac{\pi^{3/2} q}{Z_{00}(1; q^2)}, \quad (18)$$

where  $q$  is given in (17), and the generalized zeta function  $Z_{lm}$  is given in [17].

Assuming a phase shift parameterization, one can numerically invert that relation and obtain the modified energy levels, which exhibit the phenomenon of avoided level crossing by level “transmutation”.

The  $s$ -wave amplitude may be written

$$T = e^{i\delta} \sin \delta = \frac{1}{\cot \delta - i}. \quad (19)$$

We also define for convenience

$$\rho_0(s) = \frac{p^*}{\sqrt{s}} \cot \delta = \frac{2Z_{00}(1; q^2)}{L\sqrt{s\pi}}, \quad (20)$$

with the effective range parameterization near threshold

$$\sqrt{s} \rho_0(s) = \frac{1}{a_0} + \mathcal{O}(p^{*2}), \quad (21)$$

and scattering length  $a_0$ . If the first resonance is of Breit-Wigner shape, then  $\rho_0$  can be approximated linearly,

$$\rho_0(s) = \frac{1}{\gamma}(s_R - s). \quad (22)$$

Here  $s_R$  denotes the resonance position and  $\gamma$  is related to the width

$$\Gamma = \frac{p^*(s_R)}{s_R} \gamma \quad (23)$$

or the coupling constant  $\gamma = g^2/6\pi$ .

The  $N(\frac{1}{2}^-)$  ( $s$ -wave) scattering amplitude is shown in the data analysis of [36] and has an intricate behavior, becoming quickly inelastic. In a simplification of that case let us study the situation with just one elastic resonance. In that case the phase shift and elastic amplitude can be modeled where we have used a resonance mass of 1535 MeV and a width of 150 MeV. The resulting energy levels demonstrating the expected avoided level crossing are also shown in Fig. 1.

In the lower part of Fig. 1 we show the situation where the pion mass has the larger value 266 MeV. (Note that it is also used as unit mass in that plot.) The values of the stable nucleon has been set to 1068 MeV and the resonance position to 1670 MeV, all values close to the results of our calculation to be discussed in Sect. III. The coupling strength  $\gamma$  at the resonance position is unchanged.

In this setting the picture changes drastically. For our lattice size we have  $L \approx 2.68$  (in units of  $m_\pi$ ) and the energy level  $N(1)\pi(-1)$  lies clearly above the resonance. The lowest possible state is  $N(0)\pi(0)$ , which coincides

with the threshold in the non-interacting case. For attractive interaction the level moves slightly below the threshold to negative  $q^2$ , which is a finite volume artifact.

Choosing interpolators with non-zero total momentum (“moving frame”) allows in principle to obtain further energy levels and thus additional values of the phase shift. For the case of two particle of equal mass this was discussed in [19, 20] and has been used in various studies of the  $\pi\pi$ -system. The situation for pairs of hadrons with different masses is more complicated [21–23] since there even and odd partial waves may mix. In this study we rely on the case of zero momentum. Smaller quark masses will require the consideration of further  $N\pi$  operators and other interpolators.

Lüscher’s relation holds in the elastic region. Most often inelasticity sets in early due to coupled channels. An alternative approach is the inverse procedure, starting with a (unitarized) coupled channel parameterization of the scattering matrix in continuum and then determining the expected discrete energy levels on finite volumes, see, e.g., [24–27]. The lattice results for the energy levels can then be interpreted along these lines.

### III. RESULTS

#### A. Pion and nucleon, non-interacting

The masses of the free pion and the ground state nucleon  $N(\frac{1}{2}^+)$  have to be estimated with the highest possible precision in order to perform the subsequent analysis. For the gauge configurations used here the pion was studied carefully in [8, 11] where the value  $a m_\pi = 0.1673(2)$  was obtained and we use this value here as well.

For the positive parity nucleon  $N(\frac{1}{2}^+)$  we study the correlation matrix for the six operators

$$\begin{aligned} \mathcal{O}_1^+, \mathcal{O}_2^+, \mathcal{O}_3^+ &= N_+^{(1)}, N_+^{(2)}, N_+^{(3)} && \text{with } N_v = 32, \\ \mathcal{O}_4^+, \mathcal{O}_5^+, \mathcal{O}_6^+ &= N_+^{(1)}, N_+^{(2)}, N_+^{(3)} && \text{with } N_v = 64. \end{aligned} \quad (24)$$

The correlation matrix is analyzed with the variational method as discussed above. The ground state shows a stable plateau behavior in the effective energy plot Fig. 2. The first excitation is considerably higher than the expected Roper resonance. This observation is shared by other recent studies (see, e.g., [1, 4]) but disputed [2, 45]. The reason for the high value may lie in the incompleteness of the interpolator basis, i.e., possibly missing important 5-quark interpolators. To solve this puzzle is not the object of our study. Our value of the ground state nucleon (fit range 6-12) is  $a m_N = 0.672(4)$  (corresponding to  $m_N = 1068(6)$  MeV).

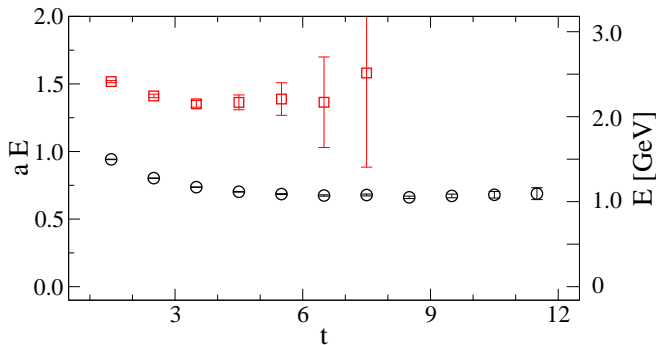


FIG. 2: The effective energy values for the  $N(\frac{1}{2}^+)$  channel (with 3-quark interpolators).

### B. Interacting $N\pi$ system

We compute the full correlation matrix for the following operators:

$$\begin{aligned}
 \mathcal{O}_1^-, \mathcal{O}_2^-, \mathcal{O}_3^- &= N_-^{(1)}, N_-^{(2)}, N_-^{(3)} && \text{with } N_v = 32, \\
 \mathcal{O}_4^-, \mathcal{O}_5^-, \mathcal{O}_6^- &= N_-^{(1)}, N_-^{(2)}, N_-^{(3)} && \text{with } N_v = 64, \\
 \mathcal{O}_7^-, \mathcal{O}_8^-, \mathcal{O}_9^- &= O_{N\pi}^{(1)}, O_{N\pi}^{(2)}, O_{N\pi}^{(3)} && \text{with } N_v = 32,
 \end{aligned} \tag{25}$$

with the definition from (4) and (6).

Let us first consider results for the subset of 3-quark interpolators  $\mathcal{O}_1^- - \mathcal{O}_6^-$ . It turns out that inclusion of the type  $N_-^{(3)}$  does not improve the quality of the diagonalization results. We therefore use only the subset  $(\mathcal{O}_1^-, \mathcal{O}_2^-, \mathcal{O}_4^-, \mathcal{O}_5^-)$ . We reproduce the usual (see, e.g. [4, 5]) pattern of energy levels (see left hand plot of Fig. 3), which have been assigned to the two  $N^*$  resonances. However, as has been observed in [46], towards smaller pion masses the lower level moves close to the expected threshold and thus lies unexpectedly low if compared to the  $N^*(1535)$ . The situation is shown in Fig. 4 (middle). The energy levels have the values 1.359(43) GeV (exponential fit, fit range 6-10) and 1.709(29) GeV (fit range 4-9).

This picture changes significantly, when one includes the  $N\pi$ -interpolators in the correlation matrix. The right hand plot of Fig. 3 shows the effective energy levels when using operators  $\mathcal{O}_1^-, \mathcal{O}_2^-, \mathcal{O}_4^-, \mathcal{O}_5^-, \mathcal{O}_7^-, \mathcal{O}_8^-, \mathcal{O}_9^-$  in the analysis. The exponential fits to the corresponding eigenvalues and the resulting energy levels are listed in Table II.

Figure 4 (right) demonstrates the difference to the previous case with only 3-quark interpolators. The lowest level now lies slightly below threshold, a feature typical for attractive  $s$ -wave [11, 12] and a finite volume artifact. This agrees with the behavior discussed in Subsect. II E. The next-higher two levels are now close to values lying approximately 130 MeV above the physical resonance positions of  $N^*(1535)$  and  $N^*(1650)$ , similar to the situation for the nucleon. Comparison with Fig. 1, where a

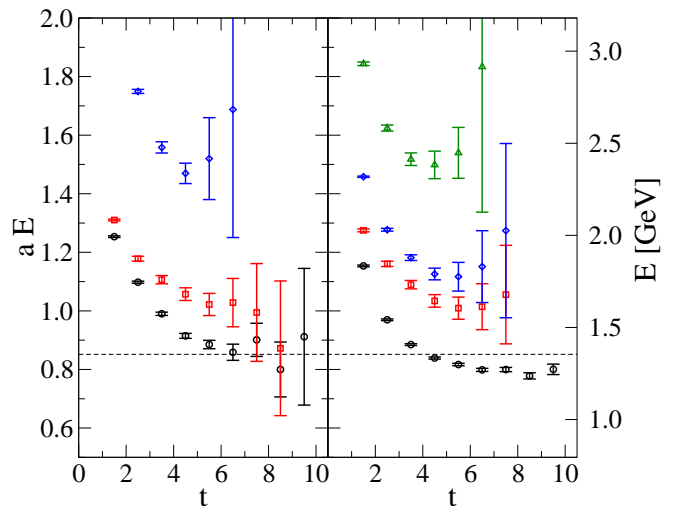


FIG. 3: Left: effective energy values for the case without  $N\pi$  contribution, right: including  $N\pi$  interpolators. The horizontal broken line indicates the threshold value  $m_N + m_\pi$ .

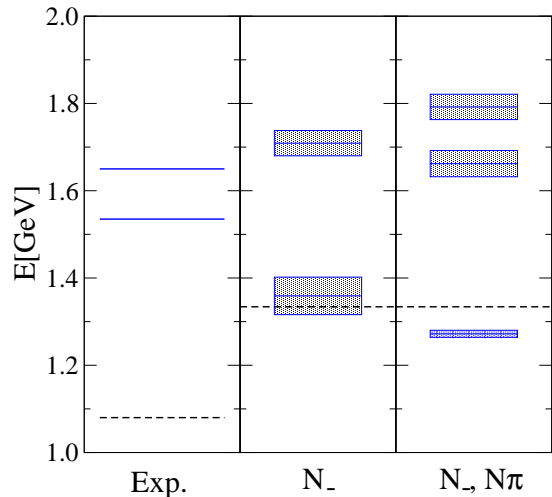


FIG. 4: Comparison of the energy levels. Left: physical mass values (experiment). Middle: result when using only 3-quark interpolators. Right: result when pion-nucleon interpolators are included. The dashed lines indicate the scattering thresholds.

single elastic resonance parameterization has been used, shows excellent agreement for the lowest two energy levels.

The eigenvectors are fingerprints of the states and one should have a stable composition across the fit range in order to be sure to identify the same eigenstate. Fig. 5 shows the eigenvector components of the three lowest eigenstates. The eigenvectors have unit norm. The absolute normalization of the 5-quark operators compared to the 3-quark ones is unclear. However, one finds that the  $\mathcal{O}_{N\pi}$  contribution to the ground state is significantly

level $n$	$t_0$	fit range	$a E_n = a \sqrt{s}$	$E = \sqrt{s}$ [GeV]	$\frac{\chi^2}{d.o.f.}$	$a p^*$	$\rho_0$	$\delta$ [degrees]
1	1	6-12	0.800(5)	1.272(8)	6.12/5	0.0985(57) i	0.149(48)	68(59)i
2	1	4-8	1.045(19)	1.662(30)	2.46/3	0.2726(155)	0.007(42)	89(9)
3	1	4-8	1.127(18)	1.792(29)	0.67/3	0.3362(134)	0.279(108)	47(10)

TABLE II: Final results for the lowest three energy levels of the coupled  $N\pi$  system with the interpolators  $\mathcal{O}_1^-, \mathcal{O}_2^-, \mathcal{O}_4^-, \mathcal{O}_5^-, \mathcal{O}_7^-, \mathcal{O}_8^-, \mathcal{O}_9^-$ . The energy levels are determined by correlated one-exponential fits to the eigenvalues  $\lambda_n(t)$  in the given fit range. We verified that two-exponential fits starting at smaller  $t$  agree with results obtained from one-exponential fits. The errors are determined by the single-elimination jackknife method. For the values given in GeV we use the lattice spacing  $a = 0.1239$  fm (Sommer parameter  $r_0 = 0.48$ fm).

larger than to the higher levels. Interpolators of type  $N_-^{(1)}$  contribute importantly to the lowest eigenstate and dominate the 3rd state, whereas the interpolators of type  $N_-^{(2)}$  are more important for the 2nd state.

In contrast, the effective energy levels of the pure 3-quark correlations system show more fluctuation. Comparing with the full  $N\pi$  system results one gets the impression that the two lowest states of the 3-quark system interpolate between the three lowest states of the complete system.

The lowest energy level of the two particle system lies below threshold and the corresponding value of  $\rho_0$  may be related to the scattering length. Table II gives also the values of  $\rho_0$  from (20) due to the Lüscher analysis and the resulting values of the phase shift, assuming elasticity. The second energy level lies close to the point where the phase shift crosses  $\pi/2$  (this value is included within the error bars). This closeness is pure chance: for slightly larger lattices this would not have been the case (cf., Fig. 1). As discussed, the kinematical situation (pion mass and lattice size) allows the assumption to be in the elastic domain and thus one is tempted to assume validity of (22). The zero of the line connecting the values of  $\rho_0$  at the two lowest energy levels give the resonance position  $a^2 s_R = 1.114(135)$  corresponding to a resonance mass  $m_R = 1.678(99)$  GeV. This is approximately 140 MeV above the physical value, but not surprising due to the unphysical pion and nucleon masses, in fact, a similar shift as for the nucleon. Also note, that the  $N\pi$  system in Nature is already inelastic and the linearity assumption not justified in that case.

The third eigenstate has a phase shift of  $47^\circ$  ( $\simeq 227^\circ$ , since the arctan is defined modulo  $180^\circ$ ), indicating a resonance lying closely above that energy value of 1.79 GeV – again assuming elastic scattering.

Due to the closeness of the threshold to the resonance in our setting, as compared to Nature, we cannot expect physical values for scattering length or decay width. With (21) we can estimate the scattering length from the point close below threshold  $s_{thr}$ . We find a value  $a_0 \simeq 5.3(\pm 1.4)$  GeV $^{-1}$  roughly four times larger than, e.g., the leading order Chiral Perturbation Theory value  $m_\pi/(4\pi F_\pi^2)$  [47, 48].

#### IV. SUMMARY

We studied  $N\pi$  scattering in the negative parity, isospin  $\frac{1}{2}$  sector in an ab initio lattice QCD calculation. The simulation parameters are: two dynamical, mass degenerate quarks, a pion mass of 266 MeV, a spatial lattice size of 1.98 fm, a volume  $16^3 \times 32$  in lattice units. We use 3-quark and meson-baryon (5 quark) interpolators and analyze the  $9 \times 9$  correlation matrix with help of the variational method.

We find a significant difference to the results of simple 3-quark correlation analyses. The overall behavior is resembling that found in meson-meson scattering lattice studies for  $s$ -wave channels [11, 12]. Due to the unphysical values of the pion mass, the resonance position is higher than the experimentally established values.

The main result of our study is that taking into account meson-baryon interpolators indeed changes the obtained energy spectrum significantly. This is a first step into that direction. Obviously this is an exploratory study and systematic uncertainties stemming from the volume size, the lattice spacing and the pion mass are not (yet) under control. More work (moving frames, different volumes, further coupled channels) will fill the gap between elastic and inelastic threshold and allow the comparison with experiment and continuum models.

#### Acknowledgments

We are grateful to Meinulf Göckeler and Akaki Rusetsky for several helpful discussions and suggestions. We would like to thank Georg Engel, Christof Gattringer, Leonid Glozman, Daniel Mohler, Colin Morningstar and Sasa Prelovsek for many discussions. Thanks also to Anna Hasenfratz for providing the dynamical configurations and to Daniel Mohler and Sasa Prelovsek for allowing us to use the perambulators derived in another project. The calculations were performed on local clusters at UNI-IT at the University of Graz. V.V. has been supported by the Austrian Science Fund (FWF) under Grant DK W1203-N16.

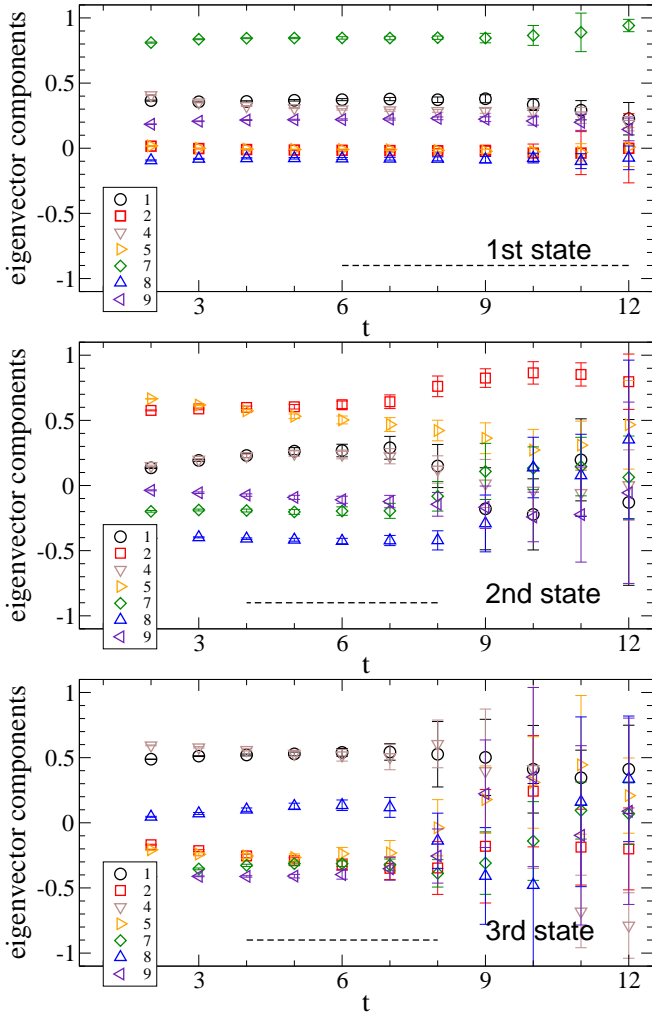


FIG. 5: The (normalized) eigenvector components for the lowest three eigenstates observed; the  $t$ -range used for the exponential fit to the eigenvalues is indicated by a broken line. In the legends the operator numbers according to (25) are given.

### Appendix A: Wick contractions

Notation for the perambulators used in this section:  $\tau(t, t', a, a', \alpha, \alpha')$  denotes the perambulator  $\tau_{\alpha\alpha'}(a, t; a', t')$  from (9), i.e., from source at  $t'$  (source vector  $a'$ , Dirac index  $\alpha'$ ) to the sink at  $t$  (source vector  $a$ , Dirac index  $\alpha$ ).

Each source/sink nucleon contributes a factor of the form  $\hat{\phi}_N(a, b, c)$ , which is constructed from the Laplacian eigenvectors. For a given time slice we have

$$\hat{\phi}_N^{snk}(a, b, c) = \sum_{\vec{x}, i, j, k} \epsilon_{ijk} v_a^i(\vec{x}) v_b^j(\vec{x}) v_c^k(\vec{x}), \quad (\text{A1})$$

where  $\epsilon$  denotes the Levi-Civita symbol,  $v$  are the Laplacian eigenvectors, and the sum runs over all sites of the time slice and over the color indices  $i, j, k$ . The corresponding factor for the pion  $\hat{\phi}_\pi(a, b)$  on a given time slice

reads

$$\hat{\phi}_\pi^{snk}(a, b) = \sum_{\vec{x}, i, j} \delta_{ij} v_a^{i*}(\vec{x}) v_b^j(\vec{x}). \quad (\text{A2})$$

By permuting and renaming the Dirac indices  $\alpha, \beta, \gamma, \dots$  and the eigenvector indices  $a, b, c, \dots$  we group the different contraction such that they have a common prefactor. There also the gamma matrices of the nucleon and pion and the parity projection operators  $P^\pm$  are located.

#### 1. $N \rightarrow N$

This entry has the form

$$\Gamma_{\alpha'\mu}^{A\dagger} P_{\mu\nu}^\pm \Gamma_{\nu\alpha}^A \Gamma_{\beta\gamma}^B \Gamma_{\gamma'\beta'}^{B\dagger} \hat{\phi}_N^{snk}(a, b, c) \hat{\phi}_N^{src}(a', b', c') \sum_{i=1}^2 A_i, \quad (\text{A3})$$

where summation over index pairs is implied.

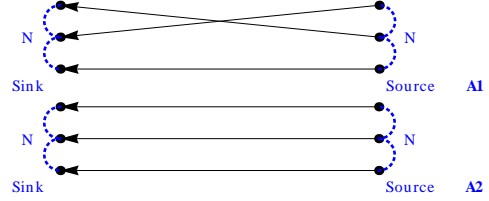


FIG. 6: Terms  $A_1$  and  $A_2$  contributing to  $N \rightarrow N$ .

$$\begin{aligned} A_1 &= \tau(t, t', c, c', \gamma, \gamma') \tau(t, t', a, b', \alpha, \beta') \\ &\quad \tau(t, t', b, a', \beta, \alpha') \\ A_2 &= -\tau(t, t', a, a', \alpha, \alpha') \tau(t, t', b, b', \beta, \beta') \\ &\quad \tau(t, t', c, c', \gamma, \gamma') \end{aligned} \quad (\text{A4})$$

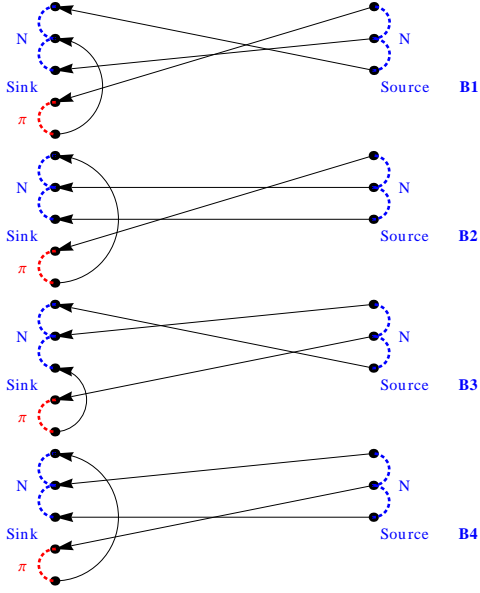
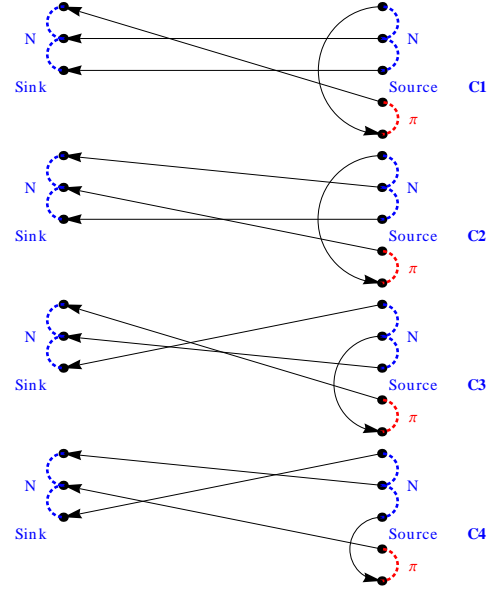
#### 2. $N \rightarrow N\pi$

This matrix element has 4 terms contributing:

$$\frac{1}{\sqrt{2}} \Gamma_{\alpha'\mu}^{A\dagger} P_{\mu\nu}^\pm \Gamma_{\nu\alpha}^A \Gamma_{\beta\gamma}^B \Gamma_{\gamma'\beta'}^{B\dagger} \Gamma_{\delta\epsilon}^\pi \hat{\phi}_N^{snk}(a, b, c) \hat{\phi}_\pi^{snk}(e, g) \hat{\phi}_N^{src}(a', b', c') \sum_{i=1}^4 B_i, \quad (\text{A5})$$

where summation over index pairs is implied.



FIG. 7: Terms  $B_1 - B_4$  contributing to  $N \rightarrow N\pi$ .FIG. 8: Terms  $C_1 - C_4$  contributing to  $N\pi \rightarrow N$ .

$$\begin{aligned}
B_1 &= 3 \tau(t, t, b, e, \beta, \epsilon) \tau(t, t', a, c', \alpha, \gamma') \\
&\quad \tau(t, t', g, a', \delta, \alpha') \tau(t, t', c, b', \gamma, \beta') \\
B_2 &= -3 \tau(t, t', b, b', \beta, \beta') \tau(t, t', c, c', \gamma, \gamma') \\
&\quad \tau(t, t, a, e, \alpha, \epsilon) \tau(t, t', g, a', \delta, \alpha') \\
B_3 &= -3 \tau(t, t, c, e, \gamma, \epsilon) \tau(t, t', b, a', \beta, \alpha') \\
&\quad \tau(t, t', a, c', \alpha, \gamma') \tau(t, t', g, b', \delta, \beta') \\
B_4 &= 3 \tau(t, t', c, c', \gamma, \gamma') \tau(t, t, a, e, \alpha, \epsilon) \\
&\quad \tau(t, t', b, a', \beta, \alpha') \tau(t, t', g, b', \delta, \beta') \quad (A6)
\end{aligned}$$

$$\begin{aligned}
C_1 &= 3 \tau(t, t', b, b', \beta, \beta') \tau(t, t', c, c', \gamma, \gamma') \\
&\quad \tau(t', t', e', a', e', \alpha') \tau(t, t', a, g', \alpha, \delta') \\
C_2 &= -3 \tau(t, t', c, c', \gamma, \gamma') \tau(t, t', a, b', \alpha, \beta') \\
&\quad \tau(t', t', e', a', e', \alpha') \tau(t, t', b, g', \beta, \delta') \\
C_3 &= -3 \tau(t, t', c, a', \gamma, \alpha') \tau(t, t', a, g', \alpha, \delta') \\
&\quad \tau(t, t', b, c', \beta, \gamma') \tau(t', t', e', b', e', \beta') \\
C_4 &= 3 \tau(t, t', a, b', \alpha, \beta') \tau(t, t', c, a', \gamma, \alpha') \\
&\quad \tau(t, t', b, g', \beta, \delta') \tau(t', t', e', c', e', \gamma') \quad (A8)
\end{aligned}$$

### 3. $N\pi \rightarrow N$

This matrix element has 4 terms contributing:

$$\begin{aligned}
&\frac{1}{\sqrt{2}} \Gamma_{\alpha'\mu}^{A\dagger} P_{\mu\nu}^{\pm} \Gamma_{\nu\alpha}^A \Gamma_{\beta\gamma}^B \Gamma_{\gamma'\beta'}^{B\dagger} \Gamma_{\epsilon'\delta'}^{\pi\dagger} \\
&\hat{\phi}_N^{snk}(a, b, c) \hat{\phi}_N^{src}(a', b', c') \hat{\phi}_\pi^{src}(g', e') \sum_{i=1}^4 C_i, \quad (A7)
\end{aligned}$$

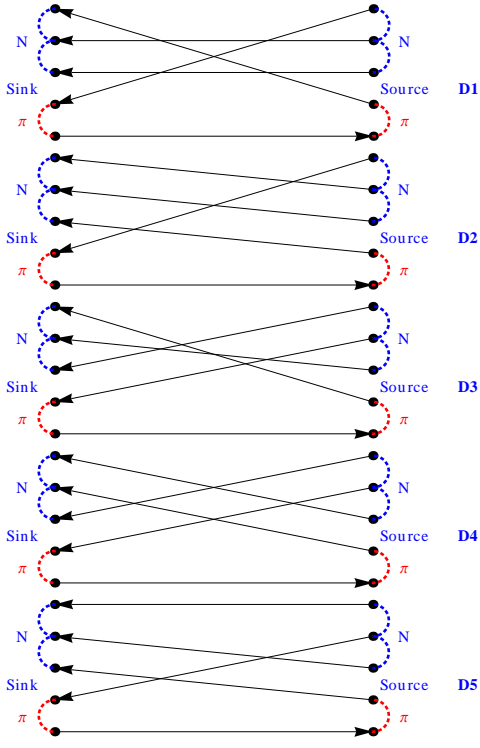
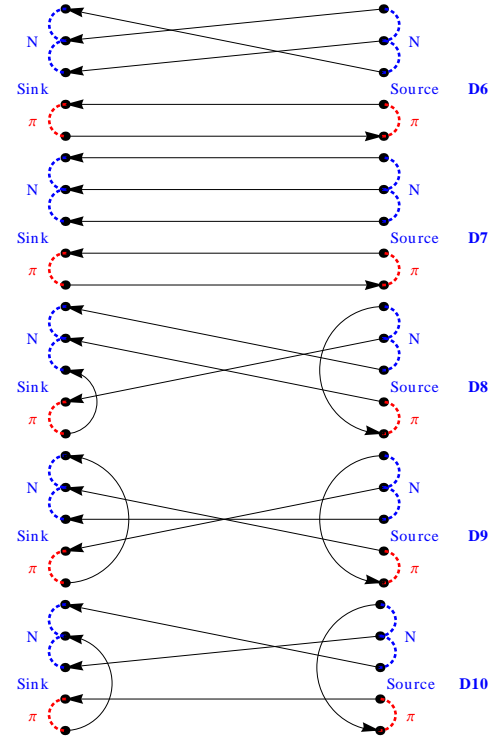
where summation over index pairs is implied.

### 4. $N\pi \rightarrow N\pi$

Here 19 terms contribute:

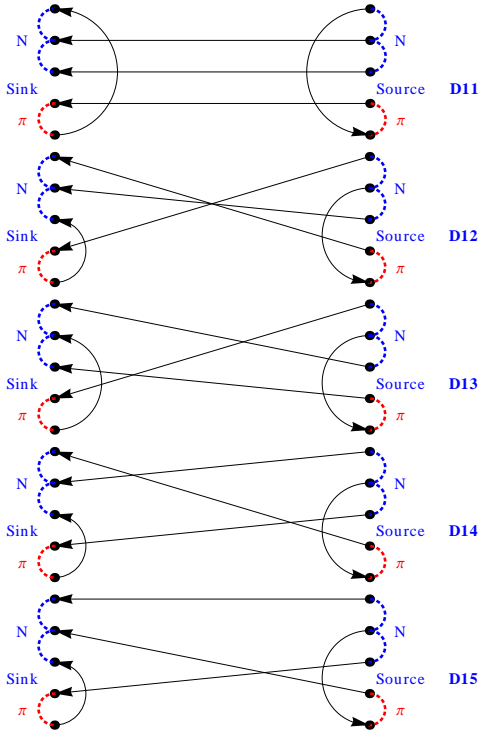
$$\begin{aligned}
&\frac{1}{2} \Gamma_{\alpha'\mu}^{A\dagger} P_{\mu\nu}^{\pm} \Gamma_{\nu\alpha}^A \Gamma_{\beta\gamma}^B \Gamma_{\gamma'\beta'}^{B\dagger} \Gamma_{\delta\epsilon}^{\pi} \Gamma_{\epsilon'\delta'}^{\pi\dagger} \\
&\hat{\phi}_N^{snk}(a, b, c) \hat{\phi}_\pi^{snk}(e, g) \hat{\phi}_N^{src}(a', b', c') \hat{\phi}_\pi^{src}(g', e') \sum_{i=1}^{19} D_i, \quad (A9)
\end{aligned}$$

where summation over index pairs is implied.

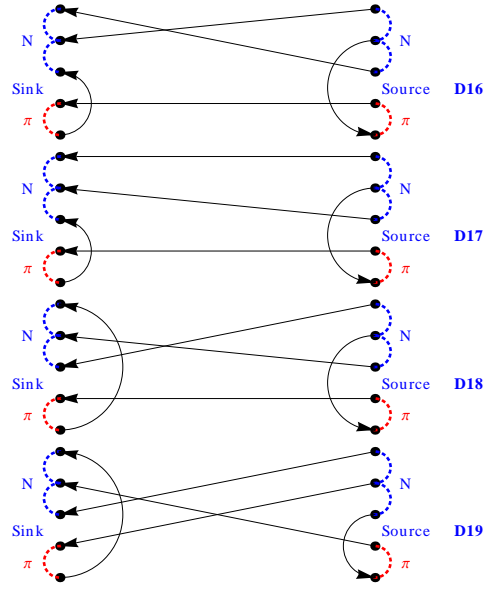
FIG. 9: Terms  $D_1 - D_5$  contributing to  $N\pi \rightarrow N\pi$ .FIG. 10: Terms  $D_6 - D_{10}$  contributing to  $N\pi \rightarrow N\pi$ 

$$\begin{aligned}
D_1 &= 3\tau(t, t', b, b', \beta, \beta') \tau(t, t', c, c', \gamma, \gamma') \\
&\quad \tau(t', t, e', e, e', \epsilon) \tau(t, t', a, g', \alpha, \delta') \\
&\quad \tau(t, t', g, a', \delta, \alpha') \\
D_2 &= -3\tau(t', t, e', e, e', \epsilon) \tau(t, t', a, b', \alpha, \beta') \\
&\quad \tau(t, t', g, a', \delta, \alpha') \tau(t, t', b, c', \beta, \gamma') \\
&\quad \tau(t, t', c, g', \gamma, \delta') \\
D_3 &= -3\tau(t', t, e', e, e', \epsilon) \tau(t, t', c, a', \gamma, \alpha') \\
&\quad \tau(t, t', a, g', \alpha, \delta') \tau(t, t', b, c', \beta, \gamma') \\
&\quad \tau(t, t', g, b', \delta, \beta') \\
D_4 &= 9\tau(t', t, e', e, e', \epsilon) \tau(t, t', a, c', \alpha, \gamma') \\
&\quad \tau(t, t', c, a', \gamma, \alpha') \tau(t, t', b, g', \beta, \delta') \\
&\quad \tau(t, t', g, b', \delta, \beta') \\
D_5 &= -6\tau(t, t', a, a', \alpha, \alpha') \tau(t', t, e', e, e', \epsilon) \\
&\quad \tau(t, t', b, c', \beta, \gamma') \tau(t, t', g, b', \delta, \beta') \\
&\quad \tau(t, t', c, g', \gamma, \delta') \tag{A10}
\end{aligned}$$

$$\begin{aligned}
D_6 &= -6\tau(t', t, e', e, e', \epsilon) \tau(t, t', g, g', \delta, \delta') \\
&\quad \tau(t, t', b, a', \beta, \alpha') \tau(t, t', a, c', \alpha, \gamma') \\
&\quad \tau(t, t', c, b', \gamma, \beta') \\
D_7 &= 6\tau(t, t', a, a', \alpha, \alpha') \tau(t, t', b, b', \beta, \beta') \\
&\quad \tau(t, t', c, c', \gamma, \gamma') \tau(t', t, e', e, e', \epsilon) \\
&\quad \tau(t, t', g, g', \delta, \delta') \\
D_8 &= -9\tau(t, t, c, e, \gamma, \epsilon) \tau(t, t', a, c', \alpha, \gamma') \\
&\quad \tau(t', t', e', a', e', \alpha') \tau(t, t', b, g', \beta, \delta') \\
&\quad \tau(t, t', g, b', \delta, \beta') \\
D_9 &= 9\tau(t, t', c, c', \gamma, \gamma') \tau(t, t, a, e, \alpha, \epsilon) \\
&\quad \tau(t', t', e', a', e', \alpha') \tau(t, t', b, g', \beta, \delta') \\
&\quad \tau(t, t', g, b', \delta, \beta') \\
D_{10} &= 9\tau(t, t', g, g', \delta, \delta') \tau(t, t, b, e, \beta, \epsilon) \\
&\quad \tau(t, t', a, c', \alpha, \gamma') \tau(t', t', e', a', e', \alpha') \\
&\quad \tau(t, t', c, b', \gamma, \beta') \tag{A11}
\end{aligned}$$

FIG. 11: Terms  $D_{11} - D_{15}$  contributing to  $N\pi \rightarrow N\pi$ 

$$\begin{aligned}
 D_{11} &= -9\tau(t, t', b, b', \beta, \beta') \tau(t, t', c, c', \gamma, \gamma') \\
 &\quad \tau(t, t', g, g', \delta, \delta') \tau(t, t, a, e, \alpha, \epsilon) \\
 &\quad \tau(t', t', e', a', \epsilon', \alpha') \\
 D_{12} &= -3\tau(t, t, c, e, \gamma, \epsilon) \tau(t, t', a, g', \alpha, \delta') \\
 &\quad \tau(t, t', g, a', \delta, \alpha') \tau(t, t', b, c', \beta, \gamma') \\
 &\quad \tau(t', t', e', b', \epsilon', \beta') \\
 D_{13} &= 3\tau(t, t, b, e, \beta, \epsilon) \tau(t, t', a, c', \alpha, \gamma') \\
 &\quad \tau(t, t', g, a', \delta, \alpha') \tau(t', t', e', b', \epsilon', \beta') \\
 &\quad \tau(t, t', c, g', \gamma, \delta') \\
 D_{14} &= 3\tau(t, t, c, e, \gamma, \epsilon) \tau(t, t', b, a', \beta, \alpha') \\
 &\quad \tau(t, t', a, g', \alpha, \delta') \tau(t', t', e', b', \epsilon', \beta') \\
 &\quad \tau(t, t', g, c', \delta, \gamma') \\
 D_{15} &= 6\tau(t, t', a, a', \alpha, \alpha') \tau(t, t, c, e, \gamma, \epsilon) \\
 &\quad \tau(t', t', e', b', \epsilon', \beta') \tau(t, t', b, g', \beta, \delta') \\
 &\quad \tau(t, t', g, c', \delta, \gamma') \tag{A12}
 \end{aligned}$$

FIG. 12: Terms  $D_{16} - D_{19}$  contributing to  $N\pi \rightarrow N\pi$ 

$$\begin{aligned}
 D_{16} &= -3\tau(t, t', g, g', \delta, \delta') \tau(t, t, c, e, \gamma, \epsilon) \\
 &\quad \tau(t, t', b, a', \beta, \alpha') \tau(t, t', a, c', \alpha, \gamma') \\
 &\quad \tau(t', t', e', b', \epsilon', \beta') \\
 D_{17} &= -6\tau(t, t', a, a', \alpha, \alpha') \tau(t, t', g, g', \delta, \delta') \\
 &\quad \tau(t, t, c, e, \gamma, \epsilon) \tau(t, t', b, c', \beta, \gamma') \\
 &\quad \tau(t', t', e', b', \epsilon', \beta') \\
 D_{18} &= 9\tau(t, t', g, g', \delta, \delta') \tau(t, t, a, e, \alpha, \epsilon) \\
 &\quad \tau(t, t', c, a', \gamma, \alpha') \tau(t, t', b, c', \beta, \gamma') \\
 &\quad \tau(t', t', e', b', \epsilon', \beta') \\
 D_{19} &= -9\tau(t, t, a, e, \alpha, \epsilon) \tau(t, t', c, a', \gamma, \alpha') \\
 &\quad \tau(t, t', b, g', \beta, \delta') \tau(t, t', g, b', \delta, \beta') \\
 &\quad \tau(t', t', e', c', \epsilon', \gamma') \tag{A13}
 \end{aligned}$$

- [1] S. Cohen *et al.*, PoS **LAT2009**, 112 (2009), [arXiv:0911.3373].  
 [2] M. S. Mahbub *et al.*, PoS **LAT2009**, 118 (2009), [arXiv:0910.2789].  
 [3] J. J. Dudek, R. G. Edwards, M. J. Peardon, D. G.

- Richards and C. E. Thomas, Phys. Rev. D **82**, 034508 (2010), [arXiv:1004.4930].  
 [4] J. Bulava *et al.*, Phys. Rev. D **82**, 014507 (2010), [arXiv:1004.5072].  
 [5] G. P. Engel, C. B. Lang, M. Limmer, D. Mohler

- and A. Schäfer, Phys. Rev. D **82**, 034505 (2010), [arXiv:1005.1748].
- [6] G. P. Engel, C. B. Lang and A. Schäfer, Low-lying lambda baryons from the lattice, 2012, [arXiv:1212.2032].
- [7] M. S. Mahbub, W. Kamleh, Waseem, D. B. Leinweber, P. J. Moran and A. G. Williams, Low-lying odd-parity states of the nucleon in lattice QCD, 2012, [arXiv:1209.0240].
- [8] C. B. Lang, D. Mohler, S. Prelovsek and M. Vidmar, Phys. Rev. D **84**, 054503 (2011), [arXiv:1105.5636].
- [9] S. Aoki *et al.*, Phys. Rev. D **84**, 094505 (2011), [arXiv:1106.5365].
- [10] X. Feng, K. Jansen and D. B. Renner, Phys. Rev. D **83**, 094505 (2011), [arXiv:1011.5288].
- [11] C. B. Lang, L. Leskovec, D. Mohler and S. Prelovsek, Phys. Rev. D **86**, 054508 (2012), [arXiv:1207.3204].
- [12] D. Mohler, S. Prelovsek and R. M. Woloshyn, Phys. Rev. D **87**, 034501 (2013), [arXiv:1208.4059].
- [13] C. Pelissier and A. Alexandru, Resonance parameters of the  $\rho$ -meson from asymmetrical lattices, 2012, [arXiv:1211.0092].
- [14] J. J. Dudek, R. G. Edwards and C. E. Thomas, Energy dependence of the  $\rho$  resonance in  $\pi\pi$  elastic scattering from lattice QCD, 2012, [arXiv:1212.0830].
- [15] M. Lüscher, Commun. Math. Phys. **104**, 177 (1986).
- [16] M. Lüscher, Commun. Math. Phys. **105**, 153 (1986).
- [17] M. Lüscher, Nucl. Phys. B **354**, 531 (1991).
- [18] M. Lüscher, Nucl. Phys. B **364**, 237 (1991).
- [19] K. Rummukainen and S. Gottlieb, Nucl. Phys. B **450**, 397 (1995), [arXiv:hep-lat/9503028].
- [20] C. H. Kim, C. T. Sachrajda and S. R. Sharpe, Nucl. Phys. B **727**, 218 (2005), [arXiv:hep-lat/0507006].
- [21] Z. Fu, Phys. Rev. D **85**, 014506 (2012), [arXiv:1110.0319].
- [22] L. Leskovec and S. Prelovsek, Phys. Rev. D **85**, 114507 (2012), [arXiv:1202.2145].
- [23] M. Göckeler *et al.*, Phys. Rev. D **86**, 094513 (2012), [arXiv:1206.4141].
- [24] V. Bernard, M. Lage, U.-G. Meißner and A. Rusetsky, JHEP **08**, 024 (2008), [arXiv:0806.4495].
- [25] M. Döring, J. Haidenbauer, U.-G. Meißner and A. Rusetsky, Eur. Phys. J. **A47**, 163 (2011), [arXiv:1108.0676].
- [26] L. Roca and E. Oset, Phys.Rev. **D85**, 054507 (2012), [arXiv:1201.0438].
- [27] J. M. M. Hall, A. C. P. Hsu, D. B. Leinweber, A. W. Thomas and R. D. Young, PoS **LAT2012**, 145 (2012), [arXiv:1207.3562].
- [28] U. G. Meißner, K. Polejaeva and A. Rusetsky, Nucl. Phys. B **846**, 1 (2011), [arXiv:1007.0860].
- [29] P. Giudice, D. McManus and M. Peardon, Phys.Rev. **D86**, 074516 (2012), [arXiv:1204.2745].
- [30] Hadron Spectrum Collaboration, M. Peardon *et al.*, Phys. Rev. D **80**, 054506 (2009), [arXiv:0905.2160].
- [31] C. Michael, Nucl. Phys. B **259**, 58 (1985).
- [32] M. Lüscher and U. Wolff, Nucl. Phys. B **339**, 222 (1990).
- [33] B. Blossier, M. DellaMorte, G. von Hippel, T. Mendes and R. Sommer, JHEP **0904**, 094 (2009), [arXiv:0902.1265].
- [34] A. Hasenfratz, R. Hoffmann and S. Schaefer, Phys. Rev. D **78**, 054511 (2008), [arXiv:0806.4586].
- [35] A. Hasenfratz, R. Hoffmann and S. Schaefer, Phys. Rev. D **78**, 014515 (2008), [arXiv:0805.2369].
- [36] R. A. Arndt, W. J. Briscoe, I. I. Strakovsky and R. L. Workman, Phys. Rev. C **74**, 045205 (2006), [arXiv:nucl-th/0605082].
- [37] D. Manley and E. Saleski, Phys. Rev. D **45**, 4002 (1992).
- [38] R. Koch, Nucl. Phys. A **448**, 707 (1986).
- [39] R. E. Cutkosky, C. P. Forsyth, R. E. Hendrick and R. L. Kelly, Phys. Rev. D **20**, 2839 (1979).
- [40] Particle Data Group, J. Beringer *et al.*, Phys. Rev. D **86**, 010001 (2012).
- [41] C. McNeile, PoS **LATTICE2007**, 019 (2007), [arXiv:0710.0985].
- [42] K. Jansen, C. Michael and C. Urbach, Eur. Phys. J. C **58**, 261 (2008), [arXiv:0804.3871].
- [43] J. J. Dudek *et al.*, Phys. Rev. D **83**, 111502 (2011), [arXiv:1102.4299].
- [44] Hadron Spectrum Collaboration, L. Liu *et al.*, JHEP **1207**, 126 (2012), [arXiv:1204.5425].
- [45] M. S. Mahbub, W. Kamleh, D. B. Leinweber, P. J. Moran and A. G. Williams, Phys.Lett. **B707**, 389 (2012), [arXiv:1011.5724].
- [46] G. P. Engel, C. B. Lang, D. Mohler and A. Schäfer, QCD with two light dynamical Chirally Improved quarks: baryons, 2013, [arXiv:1301.4318].
- [47] S. Weinberg, Phys. Rev. Lett. **17**, 616 (1966).
- [48] Y. Tomozawa, Nuovo Cim. **A46**, 707 (1966).